

**Rapid and efficient synthesis of core-shell nano formulation and nanoparticles
using 3D printed microfluidic reactor.**

by

Lili Chen

A dissertation submitted to the Graduate Faculty of
Auburn University
in partial fulfillment of the
requirements for the Degree of
Master of Material Science

Auburn, Alabama
August 3, 2019

Keywords: microfluidic, core/shell, nanoparticle, 3D printing, synthesis

Copyright 2019 by Lili Chen

Approved by

Pengyu Chen, Chair, Assistant Professor of Materials Engineering
Edward Davis, Assistant Professor of Materials Engineering
Xiaoyuan Lou, Associate Professor of Materials Engineering

Abstract

Nowdays, 3D printed microfluidics have become very popular because of their fast-printed process, highly efficient reaction and economic cost. They have been widely applied in the biology, pharmacology, chemicals, material engineering and many other fields. This thesis aims to apply microfluidic reactor in the synthesis of gold/silver core/shell nanoparticles and explore other applications of 3D printed microfluidics.

In the first and second part, the core/shell nanoparticles and 3D printing technology will be introduced in general. The definition, clarifications and applications are also mentioned. For the chapter three, the application of 3D printed microfluidic, such as centrifuge device, chemical gradient device and reacting mixers are all involved. In the chapter four, the synthesis of gold/silver core/shell nanoparticles using 3D printed microfluidic will be presented in detail. Finally, the conclusion and the challenges will be written in the chapter five.

Acknowledgments

In a twinkling of an eye, I have been studying in the United States for two years. This paper is a summary of my two years' study. First of all, I would like to thank my advisor Dr. Pengyu Chen. He always teaches me enthusiastically and patiently. In the past two years, I have learned a lot from him. In the future, he will always be my advisor and example for study and life. At the same time, I would like to thank my committee members sincerely. Thanks Dr. Edward Davis and Dr. Xiaoyuan Lou.

In addition, I want to give thanks to my friends: Wen Yang, who always enthusiastically takes to do SEM and TEM; Jiachen He, he helps me a lot in the course study; Yuxin Cai, an interesting cool guy; Xiong Feng, he teaches me a lot about the synthesis; Zhengyang Gu, I learn how to use 3D printer from him; Yuan Gao, a silent cool guy.

Table of Contents

Abstract	ii
Acknowledgments.....	iii
List of Tables	vi
List of Illustrations	vii
Chapter 1 Introduction of core/shell nanoparticles.....	1
1.1 Definition of core/Shell Nanoparticles	1
1.2 Synthesis of core/shell nanoparticles	2
1.3 Core/shell nanoparticles in biomedical application	4
1.3.1 General process of drug delivery	6
1.3.2 Core/shell nanoparticles in bioimaging application.....	6
1.3.3 Core/shell nanoparticles in sensors application	7
1.4 Core/shell nanoparticles in catalyst application.....	8
Chapter 2 Three-dimensional(3D) printed microfluidic	10
2.1 Introduction of 3D printing technology	10
2.1.1 Materials for 3D printing microfluidic	12
2.2 Introduction of microfluidic	15
2.3 Passive microfluidic.....	18
2.4 Active microfluidic	19
Chapter 3. Microfluidic application in synthesis	21

3.1 Concentration gradient microfluidic	21
3.1.1 Principles of the concentration gradient microfluidic.....	22
3.1.2 Test of the concentration gradient microfluidic.....	24
3.2 Centrifuge microfluidic.....	25
3.3 Two inlet microfluidic reactor	29
Chapter 4. 3D printed microfluidic for synthesis of silver@gold core/shell nanoparticles.....	33
4.1 Material method	33
4.1.1 Chemicals.....	33
4.1.2 Microfluidic device.....	35
4.1.3 Scanning electron microscope	35
4.1.4 Transmission electron microscope.....	36
4.1.5 Ultraviolet–visible spectroscopy.....	37
4.2 Synthesis of gold/silver core/shell nanoparticles	38
4.2.1 Preparation of gold spheres.....	38
4.2.2 Synthesis of core/shell nanoparticles by using microfluidic reactor	39
4.3 Results and discussion	40
Chapter 5. Conclusion.....	46
References	48

List of Tables

Table 2-1. 3D printing commercial materials	13
Table 2-2. Performance of active microfluidic mixers recently	17
Table 2-3. Performance of recent passive microfluidic mixers	18
Table 3-1. Hagen–Poiseuille equation in the microfluidic gradient generators.....	23

List of Illustrations

Figure 1-1. General categories of core/shell nanoparticles based on the types of core and shell materials	2
Figure 1-2. Categories of nanomaterials with multifunction	4
Figure 2-1. History of printing technology	11
Figure 2-2. Fused deposition model. (FDM)	12
Figure 2-3. Stereolithography (SLA).....	12
Figure 2-4. ABS filament in the FDM 3D printer	15
Figure 2-5. Primary forms of passive microfluidics	19
Figure 2-6. Categories of active microfluidic mixers	20
Figure 3-1. Left is the 5 concentrations gradient microfluidic (PLA), Right is the solidwork image	22
Figure 3-2. Assembly sketch	24
Figure 3-3. Solution collected from 5 outlets	24
Figure 3-4. UVVIS images of CuCl_2 solutions	25
Figure 3-5. a) Image of the microfluidic centrifugal device that filed with blue solution; b) components of the device; c) principle and mechanism in the device	27
Figure 3-6. Image of the centrifuge microfluidic	27
Figure 3-7. UVVIS of gold colloidal solution (before and after centrifuge)	28
Figure 3-8. Process of synthesis of BSA/Cu (DDC) ₂ NPs	31

Figure 3-9. The influence of the flow rate on the drug concentration and loading efficiency ..	31
Figure 3-10. The influence of the flow rate on the particle size and PDI.....	32
Figure 4-1. Primary used chemicals a) Hydrogen tetrabromoaurate (III) hydrate (HAuCl ₄) b) L-Ascorbic Acid (AA) c) Hexadecyltrimethylammonium bromide (CTAB) d) Silver nitrite (AgNO ₃) e) Stainless-steel needles.....	34
Figure 4-2. a) 3D printer b) PLA filament	35
Figure 4-3. JEOL 7000F Scanning electron microscope in Wilmore Laboratories, Auburn University.....	36
Figure 4-4. Zeiss EM10 Transmission electron microscope in Pharmaceutical Research Building, Auburn University	37
Figure 4-5. Ultrospec 2100pro Ultraviolet–visible spectroscopy.....	38
Figure 4-6. Accuspin Micro 17 Centrifuge.....	39
Figure 4-7. Assembly device	40
Figure 4-8. The left image is the UVVIS of gold nanoparticles reduced by stainless steel; the right is the SEM image	41
Figure 4-9. Stability test of the gold nanoparticles	42
Figure 4-10. UVVIS images of the core/shell nanoparticles at different mass ratios of the gold to silver.....	44
Figure 4-11. TEM image of core/shell nanoparticles	44
Figure 4-12. Stability test for one week	45

Chapter 1. Introduction of core/shell nanoparticles

Core-shell nanoparticles are more attractive than other nanoparticles because they contain new and improved properties. In the last few decades, there appears a wide variety of core/shell nanoparticles and are applied in a wide range of fields, such as biomedical, pharmaceutical, optics, and catalysis ^[1]. They all show specific properties that the traditional ones don't possess.

Core/shell structure nanoparticles possess modified properties as highly functional materials. Normally, if the materials of core or shell are different, the properties of the core/shell nanoparticles will bring substantial change. Their properties can be changed by the composition or the mass ratio of core to shell ^[2].

The primary reason for the different properties of the core/shell is the shell material coating. For example, when the reactivity decreases or the thermal stability changes, the overall stability and dispersibility of the core particles will be improved. Finally, the materials of core and shell will interact with each other. Then lead to the distinct properties ^[3].

1.1 Definition of core/shell nanoparticles

Nanoparticles can be divided into three main categories (simple nanoparticles, core/shell nanoparticles and composite nanoparticles) based on the

materials that make them up. Simple nanoparticles consist of one simple material, like gold nanoparticles, silver nanoparticles, silicon nanoparticles and so on. Core/shell nanoparticles and composite nanoparticles are both made from two or more materials. Generally, core/shell nanoparticles are composed of a core (inner layer material) and a shell (outer layer material). The material of inner layer could be organic or inorganic. The outer layer could also be organic or inorganic. So, the combination of the inner and outer layers is varied. Normally, the materials of core/shell will be dependent on the specific applications and usages [4].

According to different schedules, the core/shell nanoparticles can be classified differently. From the composition of the structure, the core/shell structure can be divided to core/shell, hollow core/shell and rattle core/shell nanostructures. The classification is shown in the figure 1-1. (a) is core/shell, (b) is hollow core/shell and (c) is rattle core/shell structure.

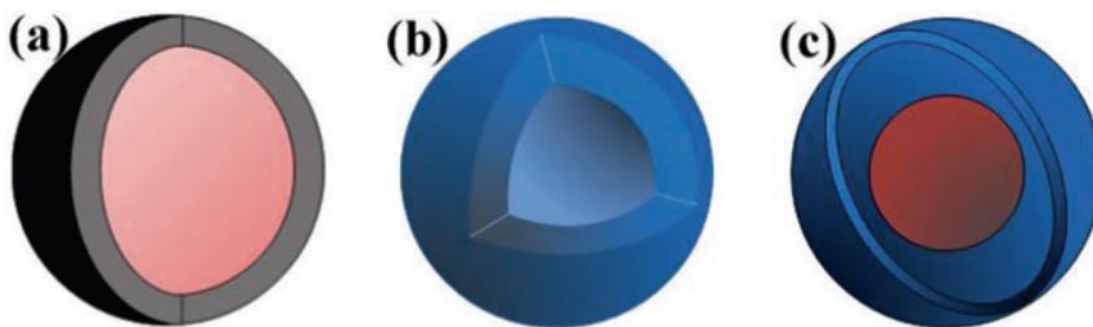


Figure 1-1. General categories of core/shell nanoparticles based on the types of core and shell materials [4].

1.2 Synthesis of core/shell nanoparticles

In the process of synthesizing nanoparticles, “top-down” and “bottom-up” are two main methods. The "top down" approach typically uses conventional machine shop or microfabrication methods to cut, grind and shape the material into the desired shape by using externally controlled tools. The “bottom up” method refers to the chemical properties of the materials. The chemical reaction of the molecules will lead to the formations of the nanoparticles.

Although these two methods can both synthesize nanoparticles, the “bottom up” method seems more popular than the other. Compared to the top-down method, the bottom-up method can produce much smaller nanoparticles. Also, the high accuracy, full control of the entire process and the least energy lost are all advantages of the bottom-up method that the top-down method doesn't possess ^[1].

In this thesis, the bottom-up method is applied in the experiment. For the reason that during the synthesis of the core/shell nanoparticle, the coating of the shell material should be uniform. It is more convenient to control the process by using the bottom-up method.

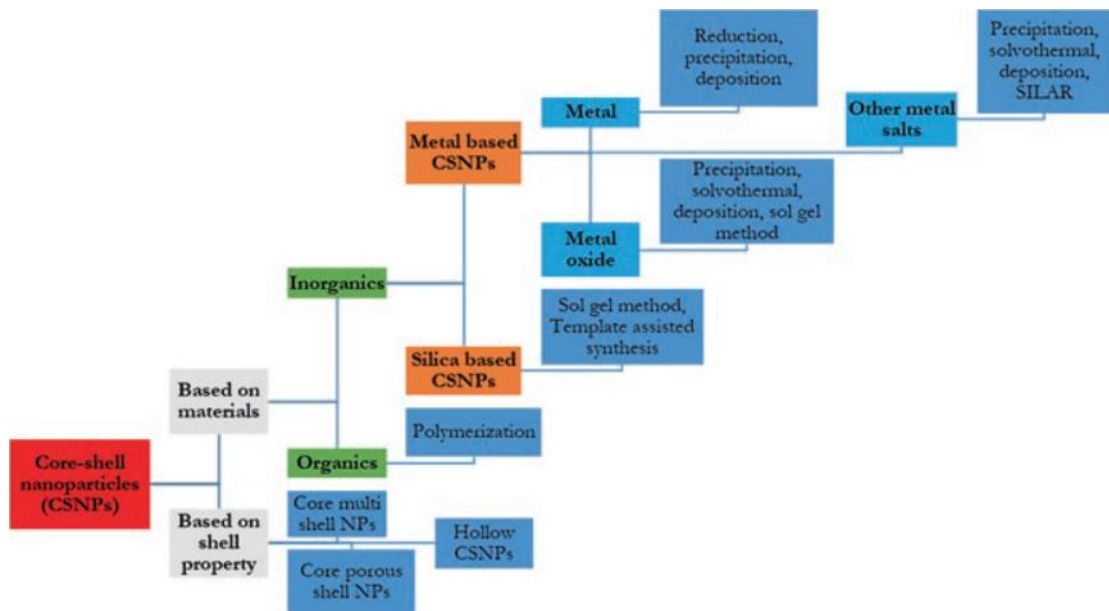


Figure 1-2. Categories of nanomaterials with multifunction ^[5]

1.3 Core/shell nanoparticles in biomedical application

Previously, there is a gap between the biology and conventional medicine. The development of the biomedical engineering filled the gap by the application of engineering skills, such as surgical diagnosis, monitoring, treatment, therapy and so on. At the same time, the synthesis and application of sub 100 nm materials make huge contributions to the fields of imaging, drug delivery and diagnostic tools.

Nanoparticles have the characteristics of small volume and high surface to volume ratio, which make them have broad application prospects in the biomedical field. In recent years, early diagnosis of various diseases such as cancer, diabetes, stroke, and Alzheimer's disease are major research hotspots in the biomedical field.

From early 1990s to 2010s, the number of papers about the nanoparticles in biomedical applications shot up. With a lot of financial resources invested in this field, nanoparticles in biomedical applications achieve great progress. Thus, many new possibilities for understanding the deep biochemical processes directly responsible for disease diagnosis and treatment have become promising ^[6].

The emergence of nanoparticles opens up new doors for research in many different fields. Also, the biomedical engineering has been affected a lot. From previous research, nanoparticles have advantages of large surface to volume ratio. It means that the nanoparticles have higher surface energy. At the same time, researchers also found that the nanoparticles have unique optical, electronic and excellent magnetic properties ^[7].

These outstanding properties are good news for the drug targeting and delivery. Since the nanoparticles have high surface to volume ratio, they can be sufficiently modified to enhance its pharmacokinetic properties, increase vascular cycle life and increase bioavailability, particularly in biomedical applications. Prolonged vascular cycle life increases the efficacy of the drug. An increase in the bioavailability of the drug means that less drugs can also efficiently work. As mentioned above, its most important characteristics have attracted the attention of researchers all over the world. It has better surface modification ability, which not

only helps to target drug delivery, but also solves the dual purpose of monitoring drug release ^[8].

1.3.1 General process of drug delivery

First, the drug is encapsulated with the help of surface functionalization with a linker that specifically targets cancer cells. Then these core/shell nanoparticles reach the target cell's location. Finally, they will disintegrate and attach to the surface. It is similar with the car transport. The nanoparticles are like truck drivers to deliver goods. Furthermore, these core/shell nanoparticles can be considered as sensors by attaching fluorescent dye. In this method, they are used to track the motion trail of the binding drugs ^[4].

1.3.2 Core/shell nanoparticles in bioimaging application

"Imaging" techniques aims to promote the diagnosis, treatment and prevention of diseases. Bioimaging technology is becoming more and more important. The imaging technology has developed a lot, such as magnetic resonance imaging (MRI), positron emission tomography (PET), ultrasound and optical imaging. They are all important methods to detect early diseases and understand the basic molecular aspects of organisms. In recent years, with the development of core/shell nanostructure materials, bioimaging technology has been greatly developed.

Molecular bioimaging techniques are usually used in vivo and vitro specimens. There exist one core/shell nanoparticles that consist of quantum dots and magnetic nanoparticles. They can be applied in dual-mode of optical and MR imaging simultaneously. These core/shell nanoparticles can be doped with quantum dots or dyes. But quantum dots reveal high toxicity. In order to minimize the toxicity, the core/shell nanoparticles are formed by applying appropriate materials ^[9].

In terms of bioimaging, properties of fluorescence and photoluminescence are used in lanthanide metal groups. Generally, lanthanide metals are designed for biocompatible shells that used for imaging and inspection because lanthanide metals possess good luminescent properties. By selecting the right lanthanide dopant, such as Er, Yb or Tm, the emission spectrum can be converted to green, blue or red wavelengths with increased intensity ^[10,11,12].

1.3.3 Core/shell nanoparticles in sensors application

Biosensors are analytical devices that analyze or sense biological samples by converting biological responses into electrical signals. It is essentially a kind of biocompatible diagnostic equipment. They are able to respond to some biochemical reaction (e.g., enzyme–substrate reactions) or bimolecular interactions (antigen–antibody, receptor–ligand, nucleic acid–protein, nucleic acid–nucleic acid, metal-macromolecule). They can transfer the signals into

electronic mode so that the signals can be quantified and discretized then generate amplified and feasible output. The primary components of a biosensor are 1. the receptor 2. the transducer 3. amplifier 4. processing part 5. display units ^[13].

Standard biosensors have at least a highly specific and stable biocatalyst that can perform reaction analysis without being affected by physical parameters such as agitation, pH and temperature. The biosensors must give accuracy and reproducibility within the required range.

Currently, magnetic nanoparticles coated with metals, silica and polymers are widely used in bioanalytical sensors. One important finding is that Au/Ag core/shell nanoparticles could be used to detect the tumor cells in vivo ^[14].

1.4 Core/shell nanoparticles in catalyst application

In providing fuels, fine chemicals, pharmaceuticals and improve the environment, the catalysis plays an indispensable role. Generally, over 90% of the chemical reactions are relied on the catalysis. So, in order to benefit the chemical industry, it is necessary to improve the catalysis activity and selectivity.

In homogeneous and heterogeneous catalysis, fine particles have a large surface to volume ratio and a special binding site, which is one of the driving forces for the development of nanoparticle catalysts ^[15].

In some papers, researchers found that the surface coating with functional materials will greatly influence the catalysts properties of the core/shell nanoparticles^[16,17].

Chapter 2. Three-dimensional(3D) printed microfluidic

2.1 Introduction of 3D printing technology

Three-dimensional (3D) printing is a manufacturing process that converts a three-dimensional computer design into a physical model by applying an additive pattern to the material using print heads, nozzles, or other mechanisms [18,19]. Originally, the concept of 3D printing was evolved from the woodblock printing. It appeared around the year 200 in China. The development history was shown in the figure 2-1. Woodblock printing is one method that emboss patterns into a block of wood. Then it was repeated until the imprint on a substrate [20]. In addition, the most common two fabrication methods are fused deposition modeling (FDM) and stereolithography (SLA), including the conversion of digital 3D designs to 2D slices for hierarchical construction [21].

Fused deposition modeling is a 3D printing technology that widely known for its speed, accuracy and competitive cost. Figure 2-2 shows the general structure of the FDM. Usually, FDM contains one nozzle, thermo-plastic filament and one build plate. The filament will be melted by the nozzle and then solidification on the build plate to form the pre-set 3D model.

In the figure 2-3, the overall components of the stereolithography (SLA) is shown. SLA is also one popular 3D printing technology. It uses beam of light to

irradiate the chemical monomers to form the polymer. The polymer will be formed layer by layer to produce the 3D model.

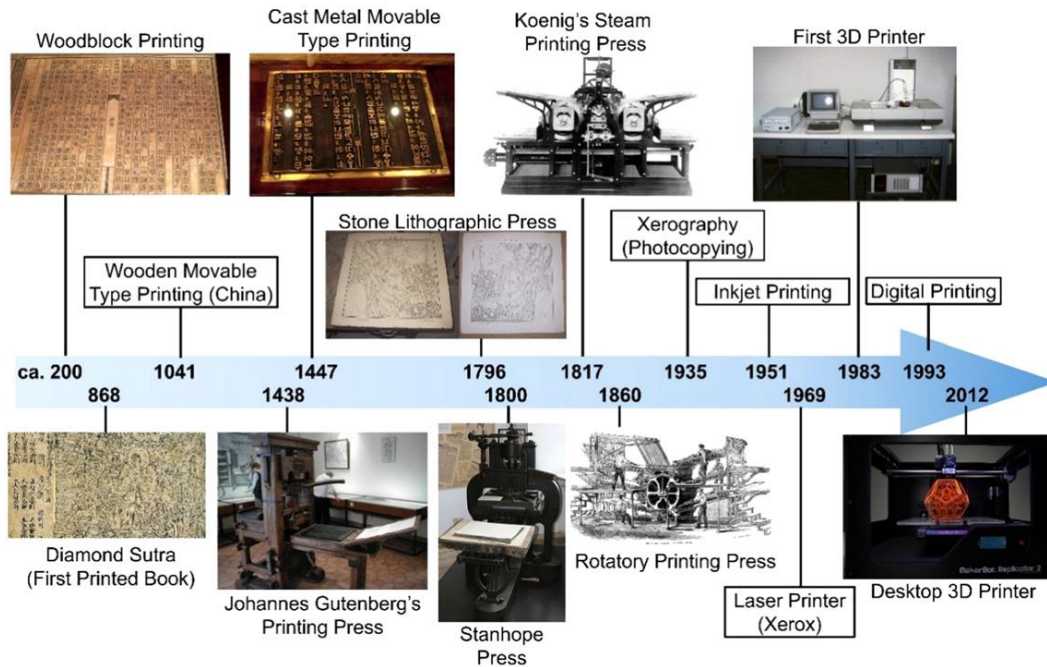


Figure 2-1. History of printing technology. Engraving is the earliest printing technology, it first appeared around 200. The first printed book had the age of 1100 years. The development of printing led to the prosperous progress of movable type printing and printing, including Johannes Gutenberg's printing, lithography, Stanhope printing, Koenig's steam printing and rotary printing. In 1983, Chuck Hall innovated the first 3D printer [20].

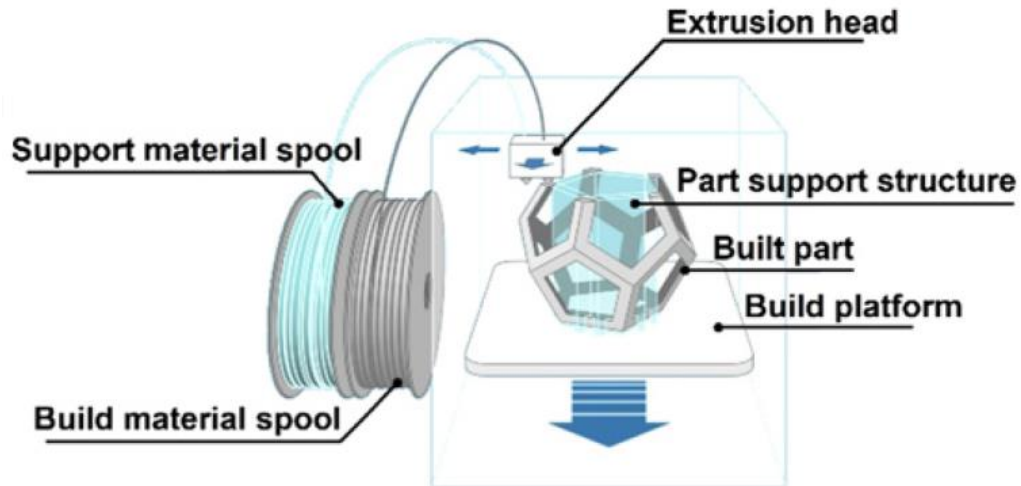


Figure 2-2. Fused deposition model. (FDM) ^[20]

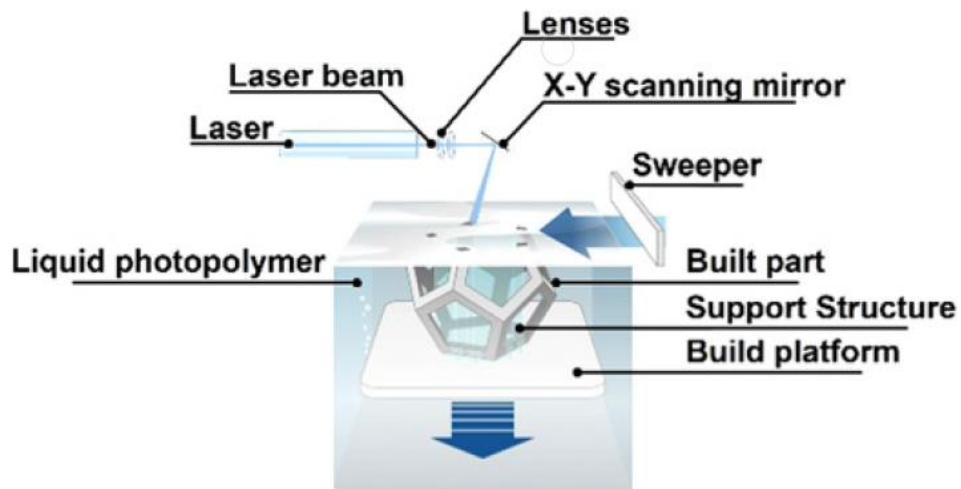


Figure 2-3. Stereolithography (SLA) ^[20]

2.1.1 Materials for 3D printing microfluidic

Understanding the performance of 3D printed materials is of great significance for the preparation, post-processing and application of 3D printed microfluidics. The choices of materials are also important, because that the

availability of new materials have not yet been standardized. Given the fact that we have not yet reached this standard, the properties of current applied 3D printing microfluidic materials will be discussed here. Table 2-1 shows the mostly used 3D printing commercial materials.

Company (Printer)	Material	Elastic modulus (GPa)	Tensile strength (MPa)	Transparency
N/A	PDMS (Sylgard 184)	0.001 32-0.002 97	3.51-7.65	Standard for comparison
MakerBot	Polyactic acid	3.368	56.6	Available
	Acrylonitrile butadiene styrene (ABS)	1.807	28.5	Unavailable
Formlabs	Polymethyl methacrylate	2.7	61.5	Available
Asiga (Pico Plus)	PlasCLEAR polypropylene/acrylonitril-butadien-styrol	—	52.6	Available
Stratasys (Objet Connex 350)	Objet Vero White Plus	2-3	50-65	Opaque, However, the objet series offers a transparent material.
	Isobornyl acrylate (15%-30%)			
	Acrylic monomer (15%-30%)			
	Urethane acrylate (15%-50%)			
	Epoxy acrylate (5-10; 10%-15%)			
	Acrylic monomer (5-10; 10%-15%)			
	Acrylic oligomer (5-10; 10%-15%), and photoinitiator (0.1-1; 1%-2%)			
3DSystems (Projet HD3500)	VisiJet M3 acrylonitrile butadiene styrene	0.866-2.168	20.5-49	Available
Somos	WaterShed XC (Proprietary)	2.77	50.4	Available
MiiCraft	Modified acrylate 5%-30%	—	—	Available
	Modified acrylate oligomer 5%-30%			
	Acrylate monomer 20%-60%			
	Epoxy monomer 5%-30%			
	Photoinitiator & additives 2%-10%			

Table 2-1. 3D printing commercial materials

Biocompatibility, transparency, printability, viscosity, and modulus of elasticity are the most considerable properties, allowing researchers to select the most appropriate material for their 3D printing products. Elastic modulus is the mechanical relationship between stress and strain. The calculation of elastic modulus is especially important when designing pipes, valves, etc. Although microfluidics handles such a small amount of fluid, the pressure generated by pumping through these devices is also needed to consider. Because elastic deformation in channels or valves are essential for conditioning microfluidics [21].

In addition, the transparency of the material is also an unnegligible property to consider. In microfluidics, visual observation is necessary to ensure the flow of the reagents. PDMS is widely used in the manufacture of microfluidic devices due to its good property of transparency. However, it should be noted that due to the photopolymerization method used in SLA 3D printing, particularly in the case of using a transparent resin, there may occur a problem that the layer above the printed layer is inadvertently cured.

Typically, SLA resins are designed to polymerize at specific wavelengths, limiting cross-compatibility between resins and 3D printers. In addition, resin viscosity is an important parameter for selecting an appropriate method to remove uncured resin from the 3D printing channel. The material also decides the print resolution. The size of a single device may vary slightly depending on the material characteristics when printing on different types of 3D printers. For FDM materials, it is very important to consider the bond strength between the layers. FDM printers also require strong support materials, some of them are difficult to remove, limiting the minimum channel size ^[22]. The figure 2-4 shows one of the most used 3D print materials in the FDM. It is made of ABS. ABS possessed properties of thermostabilization , tough, strong and the great mechanical properties after shaped by the 3D printer. It is widely applied in our lab experiments.

Biological materials or chemical agents always appear in the microfluidic applications. The chemical composition of the resin is also critical. The device should be made of resin that does not react with protein or nucleic acid reagents. Resins are biocompatible materials, so they are widely used in the microfluidic applications.

Considering the good performance of existing resins and the active innovations in the field, microfluidic devices fabricated with resins have become popular. In addition, another 3D printing material named PLA (Polylactic Acid) can not be negligible. It is also widely used as printing filaments in the FDM for its eco-friendly, low cost, odorless and low-warp properties.



Figure 2-4. ABS filament in the FDM 3D printer

2.2 Introduction of microfluidic

Microfluidic devices have a considerable impact in biomedical diagnostics and drug delivery, and they are widely used in the food and chemical industries [23]. The most important property of the microfluidic is the small scale of the flow channels (channel size of around 100 nanometers to 500 micrometers). It increases the ratio of surface to volume. However, the Reynolds number ($Re=1\rho vd/r$) of the liquid flow in such a microchannel is very small. For instance, in a typical water-based microfluidic system, the Reynolds number is about 0.1, the channel width is 100 μm , the liquid flow rate is 1 mm/s, the fluid density is 1 g/cm^3 , and the viscosity is 0.001 $\text{N s}/\text{m}^2$. Therefore, turbulent mixing is not prone to occur. That is why an efficient design of microfluidic mixing is needed to make sure when species mix in a short channel [23].

In order to promote the efficiency of the diffusive mixing effect, increasing the contact area between the species is one good method. Therefore, previous studies have proposed an approach that the sample passes through discrete via holes, cantilever plate valves, or multiple channel inputs in a microfluidic device. Another method is to increase the contact area between the mixing species by designing the microchannel structure. It helps the mixing species fold multiple times as if it flows long distance. In a passive mixing device, the sample can typically be mixed in 55-300 ms. In addition to increasing the contact area, it is also possible to improve the mixing performance by increasing the contact time between the multiple components. However, such designs will

lead to low efficiency. The table 2-2 shows the performance of active micromixers in recent five years. It can prove it.

Categories	Mixing Technique	Mixing Time (ms)	Mixing Length (μm)	Mixing Index
Acoustic/Ultrasonic	Acoustically driven sidewall-trapped microbubbles	120	650	0.025
	Acoustic streaming induced by surface acoustic wave	600	10,000	0.9
Dielectrophoretic	Chaotic advection based on Linked Twisted Map	-	1000	0.85
Electrokinetic time-pulsed	Chaotic electric fields	100	Width * 5.0	0.95
	Periodic electro-osmotic flow	-	200	0.88
Electrohydrodynamic force	Staggered herringbone structure	-	825	0.2
	Staggered herringbone structure	-	2300	0.5
Thermal actuation	Thermal	-	6000	-
Magneto-hydrodynamic flow	High operating frequency	1100	500	0.977
Electrokinetic instability	Low Reynolds number	-	1200	0.98
	Low Reynolds number	-	1200	0.98

Table 2-2. Performance of active microfluidic mixers recently ^[24]

Table 2-3 lists the performance of recent passive microfluidic mixers. Compared to the passive mixing scheme, the active mixing scheme specifically designs the microchannel structure to increase the contact area or contact time (or both) of multiple species, and the active mixing scheme accelerates the diffusion process by applying an external force to the sample. In general, active mixing are accomplished by using micromachining techniques to incorporate some form of mechanical sensor into the microfluidic device ^[24].

Categories	Mixing Technique	Mixing Time (ms)	Mixing Length (μm)	Mixing Index
Lamination	Wedge shaped inlets	1	1	0.9
	90° rotation	-	-	0.95
Zigzag channels	Elliptic-shape barriers	-	10,000	0.96
3-D serpentine structure	Folding structure	489	-	0.01
	Creeping structure	-	-	0.015
	Stacked shim structure	-	-	-
	Multiple splitting, stretching and recombining flows	-	-	-
	Unbalanced driving force	-	815 ψ	0.91
Embedded barriers	SMX	-	-	-
	Multidirectional vortices	-	4255	0.72
Twisted channels	Split-and-recombine	730	96,000	~1
Surface-chemistry	Obstacle shape	-	1000	0.98
	T-/Y- mixer	-	1000	0.95

Table 2-3. Performance of recent passive microfluidic mixers ^[24]

2.3 Passive microfluidic

The passive micromixer has no moving parts, and with no energy put in except the indenter for driving a fluid to flow at one constant speed. Due to the inherent laminar flow, the mixing in passive mixers relies primarily on chaos that achieved by controlling laminar flow within the microchannels or enhancing molecular diffusion by increasing the contact area and contact time. The figure 2-5 exhibits the primary forms of passive microfluidics.

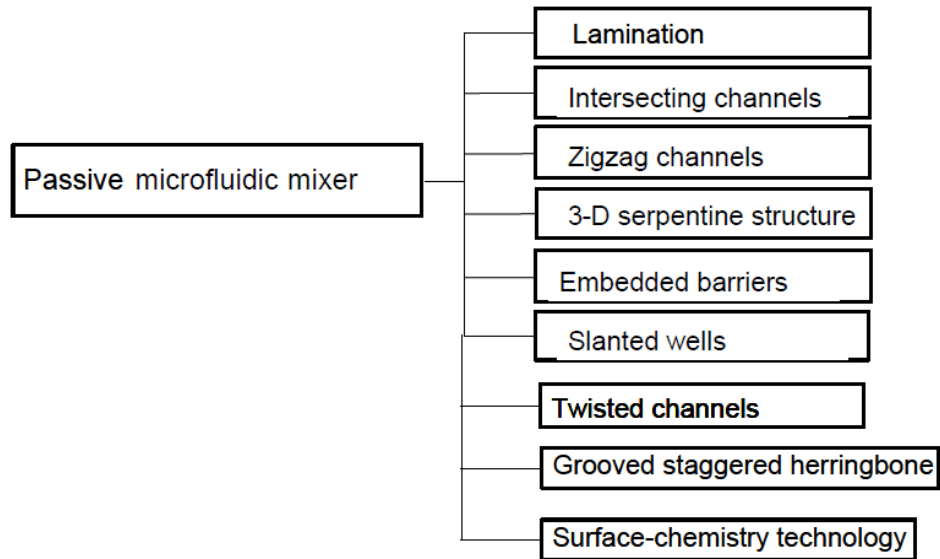


Figure 2-5. Primary forms of passive microfluidics

2.4 Active microfluidic

Unlike passive mixers, active microfluidic mixers use some form of external energy to agitate fluid flow. The figure 2-6 gives the classifications of active mixers. From the figure, we could see the categories of active microfluidic mixers are large.

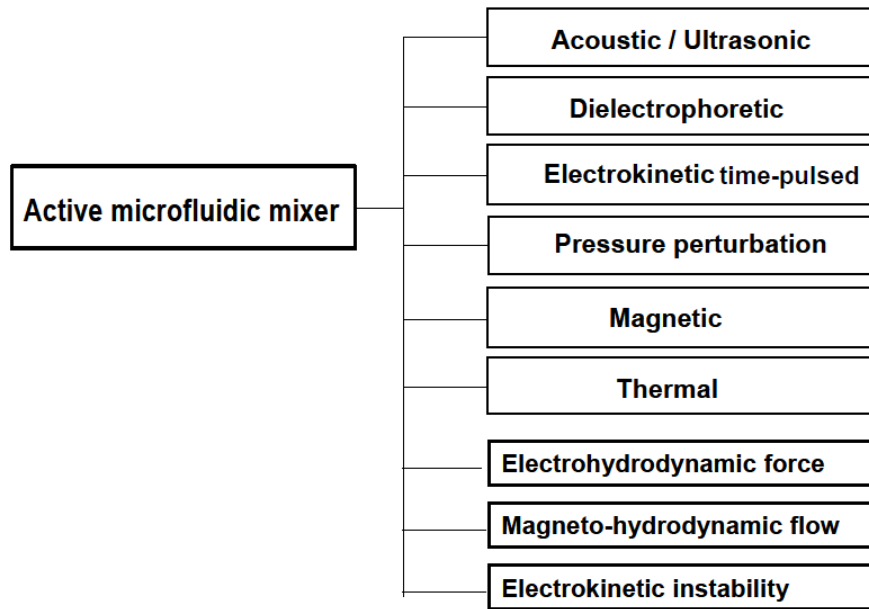


Figure 2-6. Categories of active microfluidic mixers ^[24]

Chapter 3. Microfluidic application in synthesis

In this chapter, the application of the microfluidic in the previous experiments will be introduced. Based on the previous disciplines of researches, some novel microfluidic mixers are designed and printed in our lab. It contains concentration gradient microfluidics, centrifuge microfluidics and two inlets microfluidic reactor. Also, they all show great performance in the tests.

3.1 Concentration gradient microfluidic

Concentration gradient plays an important role in the area of biomedicine, such as wound healing, immune response, cancer metastasis and so on. They all depend on the biomolecular gradients to enhance and regulate cellular signaling pathways. To understand the effects of chemical stimulation on cellular signaling pathways, scientists have been looking for other ways to artificially design the vivo cellular microenvironment [25].

In the last century, lots of biologists tried to seek methods to simulate the vivo cell microenvironment. Lots of vitro platform were produced, such as Boyden chamber, Dunn slide chamber, Zigmond chamber, etc [25].

Although much knowledge on cellular signaling pathways was studied, there are still lots of limitations of these platforms. The scales of the length and

the inner diameter are not relevant to biological cells. For most cells, their diameters range from 1 to 100 μm and secrete intercellular signals, such as cytokines and chemokines, have a concentration gradient of approximately 250 μm [26]. Under this situation, only the microfluidic platform could satisfy the requirements. That's why the microfluidic platforms become more and more popular in the new century.

3.1.1 Principles of the concentration gradient microfluidic

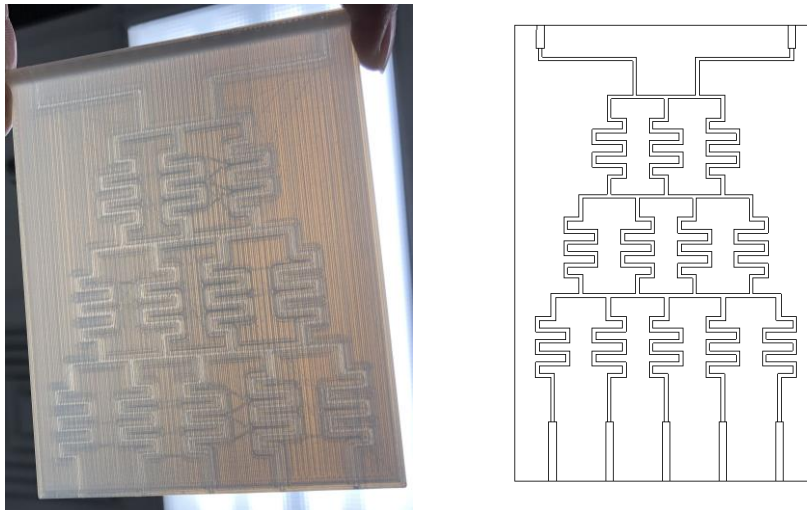


Figure 3-1. Left is the 5 concentrations gradient microfluidic (PLA), Right is the solidwork image.

This principle is from Hagen–Poiseuille [25] equation. It is used to simplify fluid flow in microfluidic into equivalent hydraulic circuits. It is similar to the electric circuits. Table 3-1 shows how this equation applied in the microfluidic.

Electric circuits	Hydraulic circuits
<p>Ohm's law:</p> <p>$V = RI$</p> <p>where V is the voltage, R is the electrical resistance and I is the electrical current</p>	<p>Hagen-Poiseuille equation:</p> <p>$\Delta P = R_f Q$</p> <p>where ΔP is the pressure drop, R_f is the hydraulic resistance and Q is the flowrate.</p>
<p>Electrical network:</p>	<p>Fluidic mixer network:</p>
<p>Encircled numbers represent current nodes.</p> <p>Kirchoff current law:</p> <p>At each node:</p> <p>Node n: $\sum_{i=1}^n I_i = 0$</p> <p>where n is the total number of branches into or out of the node.</p>	<p>Encircled numbers represent concentration nodes.</p> <p>Mass conservation:</p> <p>At each node:</p> <p>Node n: $\sum_{i=1}^n Q_i = 0$</p> <p>where n is the total number of channels into or out of the node.</p>
<p>Current division:</p> <p>Applied at nodes 1, 2 and 3:</p>	<p>Concentration division:</p> <p>Applied at nodes 1, 2 and 3:</p>
<p>Node 1: $I_3 = \left(\frac{R_2}{R_1 + R_2} \right) I_1$;</p> <p>$I_4 = \left(\frac{R_1}{R_1 + R_2} \right) I_1$</p> <p>Node 3: $I_5 = \left(\frac{R_3}{R_2 + R_3} \right) I_2$;</p> <p>$I_6 = \left(\frac{R_2}{R_2 + R_3} \right) I_2$</p> <p>Node 2: $I_4 + I_5 =$</p> $\left(\frac{R_1}{R_1 + R_2} \right) I_1 + \left(\frac{R_3}{R_2 + R_3} \right) I_2$	<p>Node 1: $Q_3 = \left(\frac{R_{f2}}{R_{f1} + R_{f2}} \right) Q_1$;</p> <p>$Q_4 = \left(\frac{R_{f1}}{R_{f1} + R_{f2}} \right) Q_1$</p> <p>Node 3: $Q_5 = \left(\frac{R_{f3}}{R_{f2} + R_{f3}} \right) Q_2$;</p> <p>$Q_6 = \left(\frac{R_{f2}}{R_{f2} + R_{f3}} \right) Q_2$</p> <p>Node 2: $Q_4 + Q_5 =$</p> $\left(\frac{R_{f1}}{R_{f1} + R_{f2}} \right) Q_1 + \left(\frac{R_{f3}}{R_{f2} + R_{f3}} \right) Q_2$ <p>Concentration flowing out of mixer module R_{f2}:</p> $C_{R_{f2}} = \frac{Q_4 \cdot C_0 + Q_5 \cdot C_1}{(Q_4 + Q_5)}$ <p>Concentration out of any mixer module is:</p> $C_{mixer\ module} = \frac{\sum_{i=1}^2 Q_i \cdot C_i}{\sum_{i=1}^2 Q_i}$ <p>where i refers to the left and right concentration streams flowing into each mixer module.</p>

Table 3-1. Hagen–Poiseuille equation in the microfluidic gradient generators [25]

3.1.2 Test of the concentration gradient microfluidic.

In order to test the reliability of this printed microfluidic, the copper (II) chloride solution was chosen as comparison medium. First, prepare 0.1M copper (II) chloride solution. Then use syringes to absorb 10 ml of DI water and 10 ml of CuCl_2 solution, respectively. Afterward, set up the syringe pump and microfluidic like the figure 3-2 show. Finally, collect the solution from the 5 outlets and test the UVVIS to compare the concentrations by their absorbance. The solutions are shown in the figure 3-3.

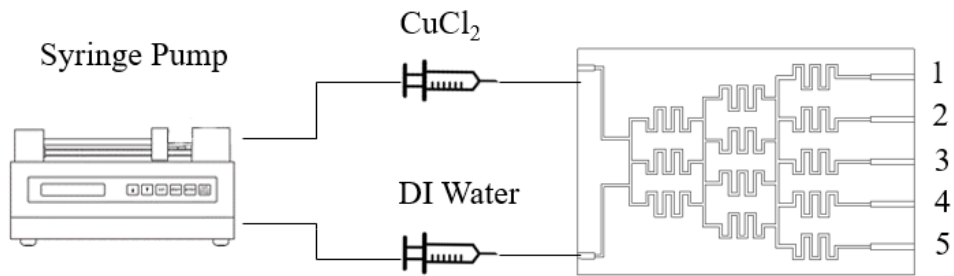


Figure 3-2. Assembly sketch

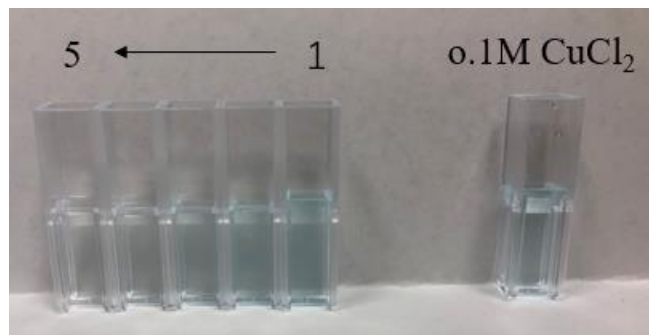


Figure 3-3. Solution collected from 5 outlets.

The figure 3-4 shows the UVVIS images of the solution collected from 5 outlets. The top line is the pure 0.1M CuCl_2 that didn't go through the microfluidic and acts as a reference. Except the top one, the lines from up to bottom are number 1 to 5 solutions. The absorbance decreases gradually, it represents the concentration gradually decreases. Although the specific concentration couldn't be got from the figure, it can still prove that the concentration gradient exists.

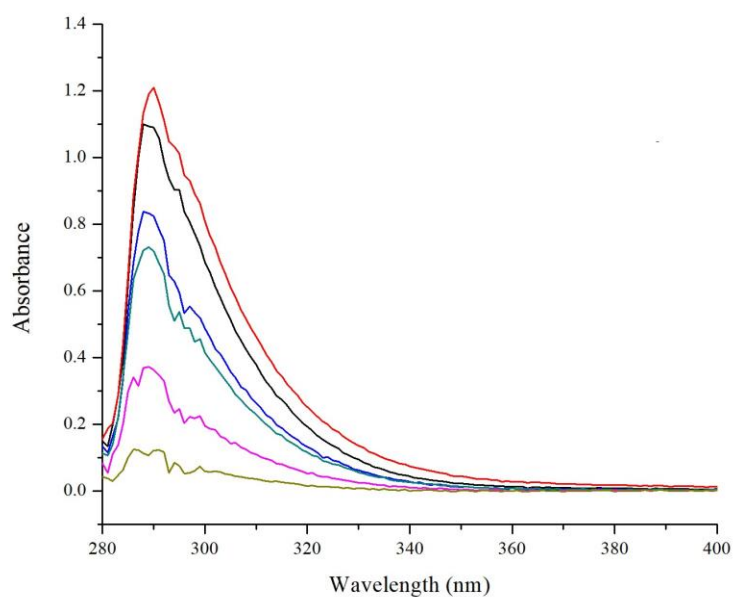


Figure 3-4. UVVIS images of CuCl_2 solutions

3.2 Centrifuge microfluidic

One central element of nanoscience and technology is separation of colloids and biomolecules. There are a variety of separation methods, such as

chromatography, field flow separation and electrophoresis, analysis of ultra-fast centrifugation technology. They all provide high resolution at the nanoscale and are widely used in biotechnology to separate cell components and macromolecular complexes ^[27]. These techniques need differential force generated by gravity or centrifugal fields on different mass objects and provide information about the size and shape of the nanoparticles and polymer complexes.

Although the traditional centrifuge is widely applied in the biotechnology or other scientific study, its existence poses a challenge to the preparation and stability during the separation process. Under this condition, some scientists come up with some new ideas that apply the microfluidics in the centrifuge. They designed the microfluidics like the figure 3-5 shows. This technique is similar to sedimentation field-flow separation (FFF) but does not require surface interaction. It is implemented by using microfluidic technology, which has a number of advantages, such as high throughput, low cost, and controlled laminar flow ^[27].

From the figure 3-5 we could see that after centrifuge, the larger particles will be separated near the outer wall of the channel. The smaller ones will be around the inner channel. This conclusion has been confirmed in other micrometer scale experiments ^{[28][29]}. But it hasn't been applied in the nanometer scale. So, I designed one centrifuge microfluidic to try. The device and results are shown in the figure 3-6 and 3-7.

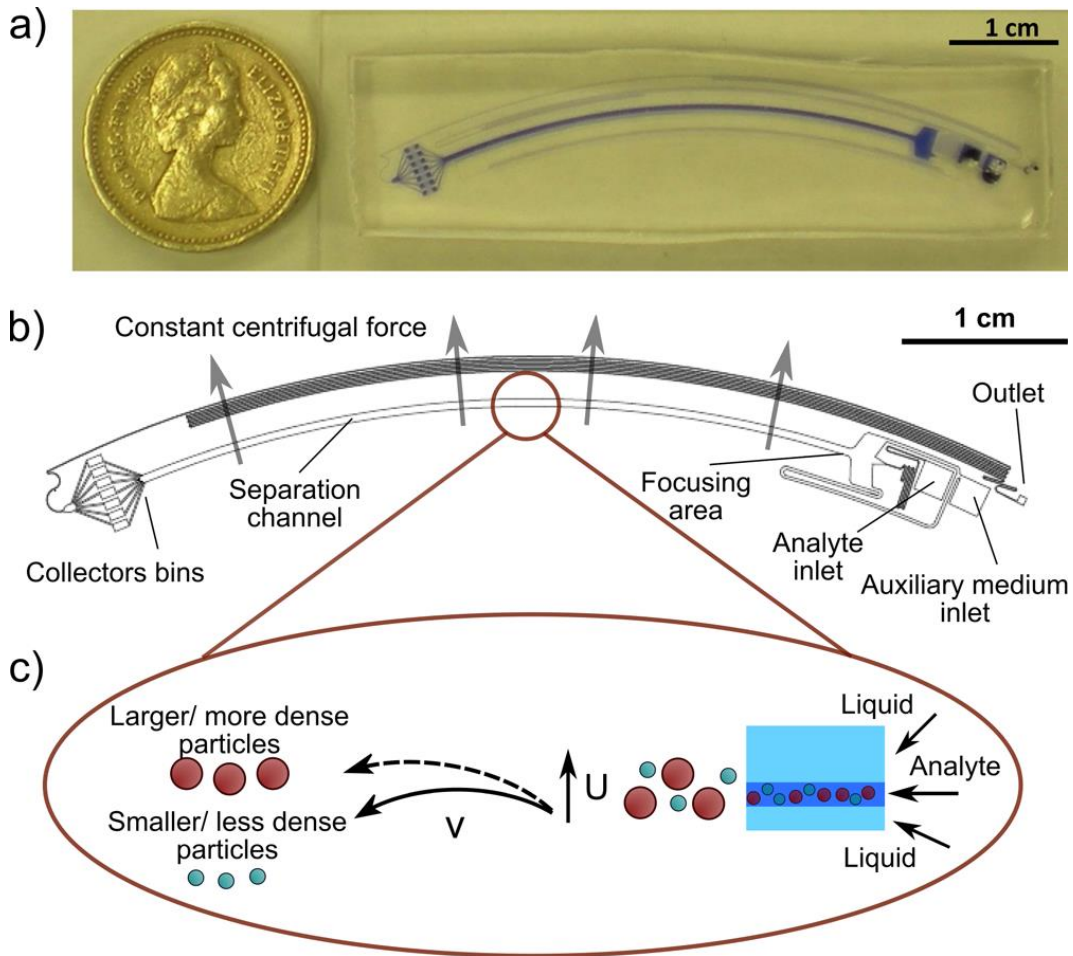


Figure 3-5. a) Image of the microfluidic centrifugal device that filled with blue solution; b) components of the device; c) principle and mechanism in the device [27].

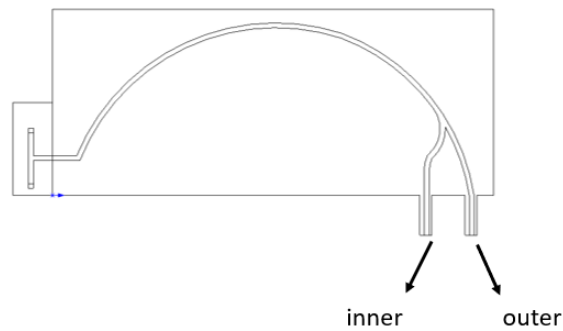


Figure 3-6. Image of the centrifuge microfluidic

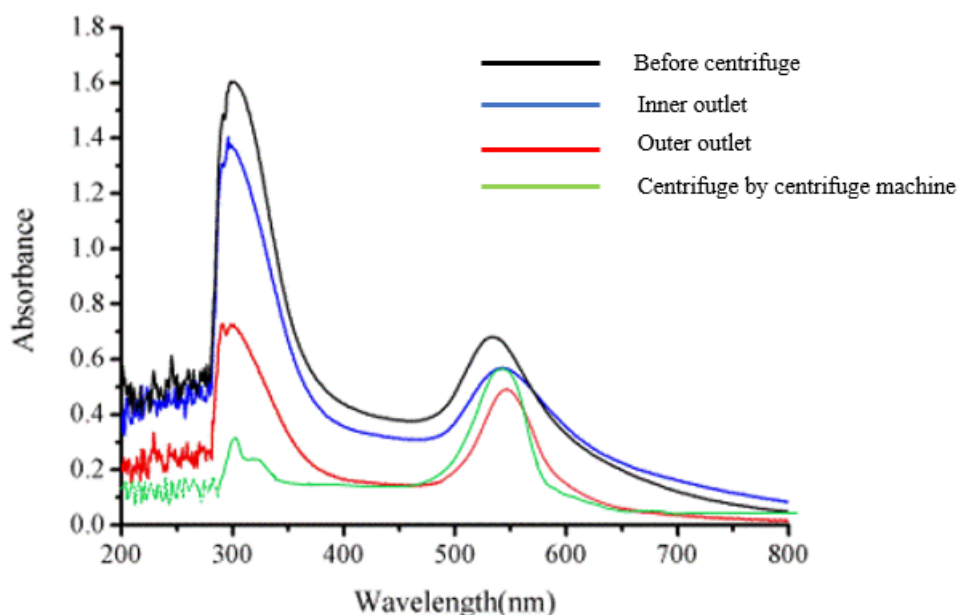


Figure 3-7. UVVIS of gold colloidal solution (before and after centrifuge).

In this experiment, I used the stainless steel as reducing agent to reduce the 10mM HAuCl_4 solution. After collect the gold colloidal solution, there are still lots of other metal ions remain in the solution except the gold nanoparticles^[30]. In order to get rid of the metal ions and archive the pure gild nanoparticles, the centrifuge is essential.

In order to compare the efficiency of the centrifuge microfluidic, the centrifuge machine is applied. From the figure 3-7 we could see that before centrifuge, the peak at the wavelength of 300 nm is sharp because of the effects of metal ions. After the centrifuge by machines, the peak will become much lower. It means that if the metals ions exist, they will form peak around 300 nm. The red line is the solution after going through the centrifuge microfluidic. Although it

still has peak around the 300 nm, it much lower than the peak before centrifuge. This may conclude that this kind of centrifuge microfluidic can partially have the effect as same as the centrifuge machine.

3.3 Two inlet microfluidic reactor

Microfluidic reactors are part of the micromachining field that handles the flow of tiny liquids in micron-sized channels. In 1990s, the microfluidic reactors were originally developed. Then after researching and promoting for 10 years, they have become widely applied in pharmaceutical, biotechnology, chemical industry and so on. For instance, chemical synthesis, diagnosis, crystallization, drug delivery, high-throughput screening and so on ^[31].

The most attractive point for the microfluidic reactor is the microscale channel. The effect of this small size is that fluid properties are increasingly controlled by viscous forces rather than inertia. Also, the Reynold number Re will decrease as the cross-sectional area of the channel decreases. So, the fluids in the channels usually tend to exhibit the status of laminar flow, it is a stable state flow, the fluids will not interact each other when they flow. What's more, due to the reduction in the size of inner channel, the surface to volume ratio increases. It also improves the heat and mass transfer efficiency ^[31].

Here, one simple two inlet microfluidic reactor is introduced. It was designed and used to synthesize BSA/Cu (DDC)₂ NPs. Cu (DDC)₂ is copper diethyldithiocarbamate that combined with Disulfiram (DSF) and copper ions, which has potent anticancer activities. However, it is hard to solute in the water, which becomes one problem for clinical application. In order to handle the problem, the bovine serum albumin (BSA) is used to coated around the surface of the Cu (DDC)₂ nanoparticles. This research was finished by Dr Feng Li, Assistant Professor in department of Drug Discovery and Development, Auburn University, and his laboratory members. And the figures are from the unpublished data in his lab.

In this research, our lab provides the 3D printed microfluidic reactor. Dr Li used the microfluidic to synthesize the BSA/Cu (DDC)₂ NPs, the figure 3-8 shows the synthesize process. The figure 3-9 shows the drug concentration can be controlled by the flow rate. The concentration and loading efficiency will increase with the increasing flow rate. Figure 3-10 shows the increasing flow rate will lead to the increasing particle size and polydispersity index (PDI). These figures all indicate that it is a controllable process by using microfluidic reactor.

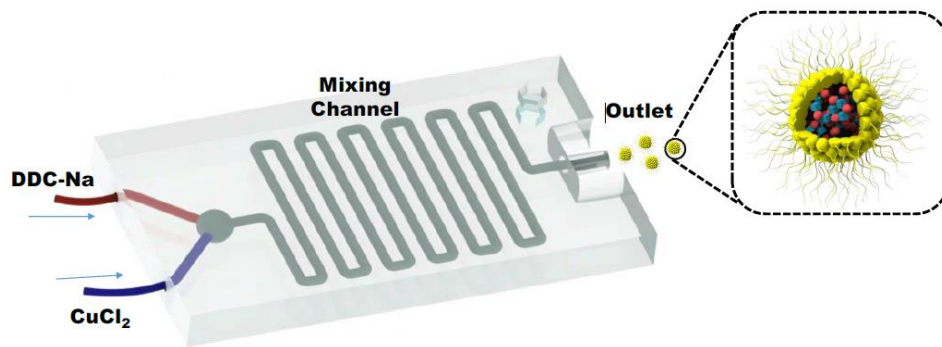


Figure 3-8. Process of synthesis of BSA/Cu (DDC)₂ NPs

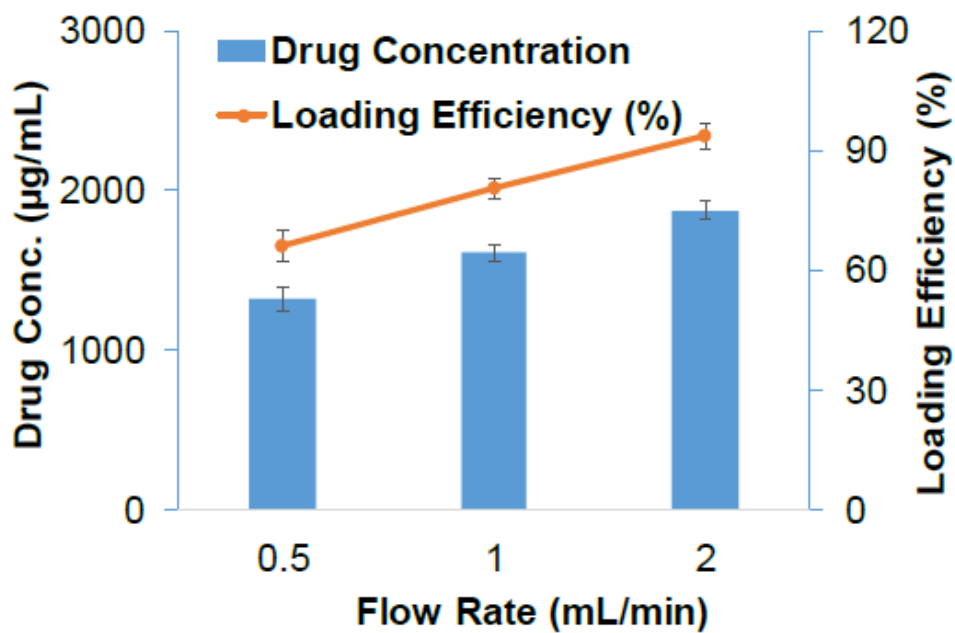


Figure 3-9. The influence of the flow rate on the drug concentration and loading efficiency

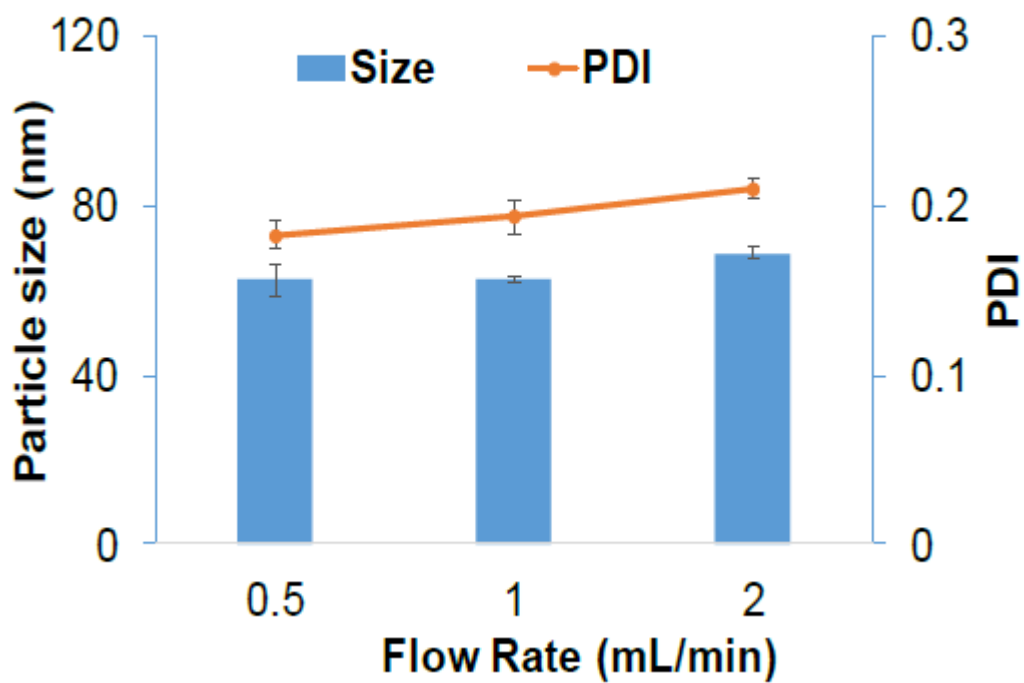


Figure 3-10. The influence of the flow rate on the particle size and PDI

Chapter 4. 3D printed microfluidic for synthesis of silver@gold core/shell nanoparticles

In this chapter, one microfluidic reactor is printed by FDM 3D printer. Then the reactor is used to synthesize silver@gold core/shell nanoparticles in a constant continuous flow rate. The nanoparticles are synthesized by using stainless steel as reducing agent, which is rapid and efficient. SEM, TEM and UVVIS are applied to observe the characteristics of the gold and core/shell nanoparticles. The experiment shows that the flow rate affects the mass ratio of the gold to silver. This process reveals the effect of different mass ratios to the core/shell structures by observing the UVVIS images. Also, it proves the flow rate can control the core/shell structure by using microfluidic reactor. It makes the synthesis process more predicable and controllable. Moreover, it shows high stability of the core/shells structure.

4.1 Material method

4.1.1 Chemicals

Hydrogen tetrabromaurate (III) hydrate (HAuCl_4) is purchased from Alfa Aesar (Tewksbury, USA). L-Ascorbic Acid (AA), silver nitrite (AgNO_3) and sodium hydroxide (NaOH) are all bought from the VWR International (Radnor, USA). Hexadecyltrimethylammonium bromide (CTAB) is bought from

Merck KGaA (Darmstadt, Germany). The stainless-steel needles are bought from McMaster-Carr company (Elmhurst, USA).

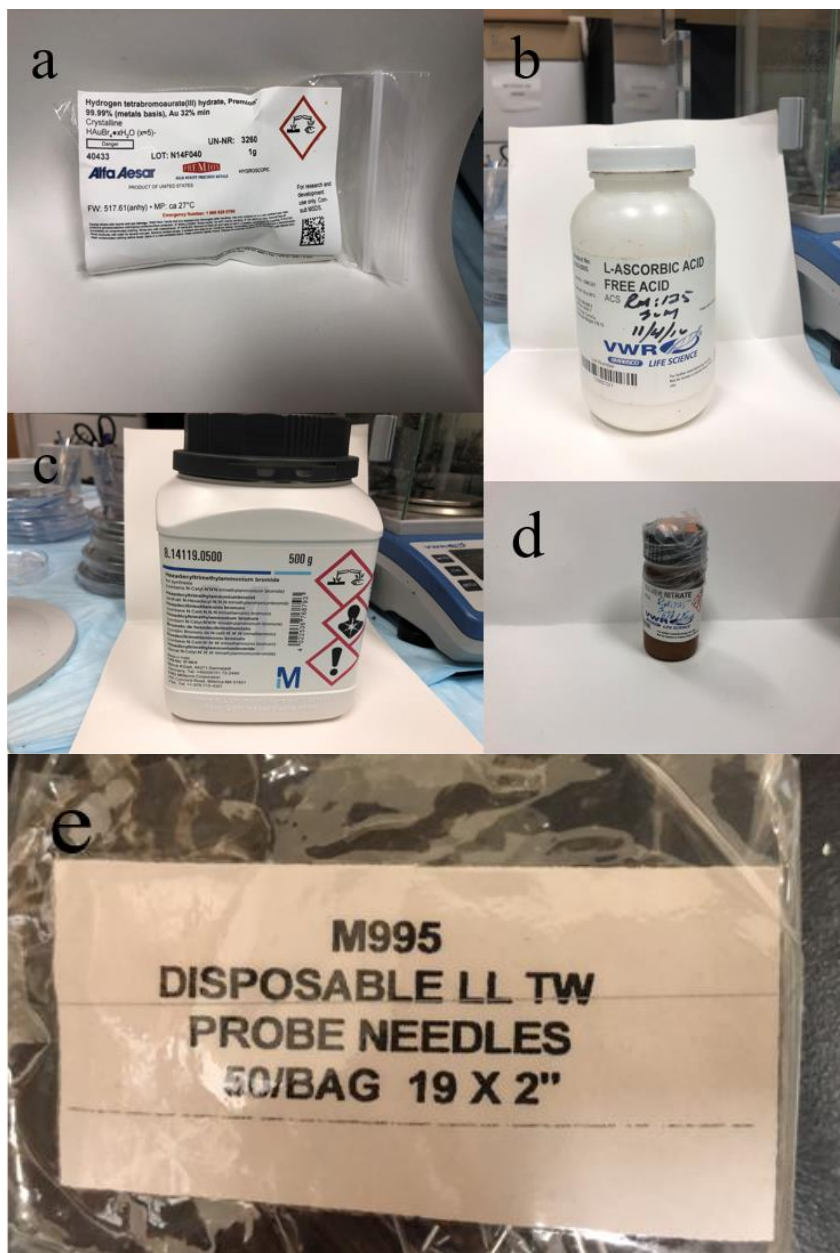


Figure 4-1. Primary used chemicals a) Hydrogen tetrabromoaurate (III) hydrate (HAuCl_4) b) L-Ascorbic Acid (AA) c) Hexadecyltrimethylammonium bromide (CTAB) d) silver nitrite (AgNO_3) e) Stainless-steel needles

4.1.2 Microfluidic device

The microfluidic reactor is printed by 3D printer using Polylactic acid (PLA) material. The 3D printer is purchased from QIDI Technology (Ruian, China). PLA filament is purchased from HATCHBOX (California, USA).



Figure 4-2. a) 3D printer b) PLA filament

4.1.3 Scanning Electron Microscope

The size and distribution of the gold nanoparticles that reduced by the stainless steel are characterized by the Scanning Electron Microscope (JEOL 7000F Scanning Electron Microscope in Wilmore Laboratories, Auburn University).



Figure 4-3. JEOL 7000F Scanning electron microscope in Wilmore Laboratories, Auburn University

4.1.4 Transmission Electron Microscope

The morphology of the gold/silver core/shell nanoparticles are characterized by Transmission Electron Microscope (Zeiss EM10 Transmission Electron Microscope in Pharmaceutical Research Building, Auburn University).



Figure 4-4. Zeiss EM10 Transmission electron microscope in Pharmaceutical Research Building, Auburn University

4.1.5 Ultraviolet–visible spectroscopy

After synthesis, the different mass ratios of gold to silver core/shell nanoparticles are tested in the Ultrospec 2100pro Ultraviolet–visible spectroscopy, comparing and studying the how the mass ratio affect the core/shell structure.

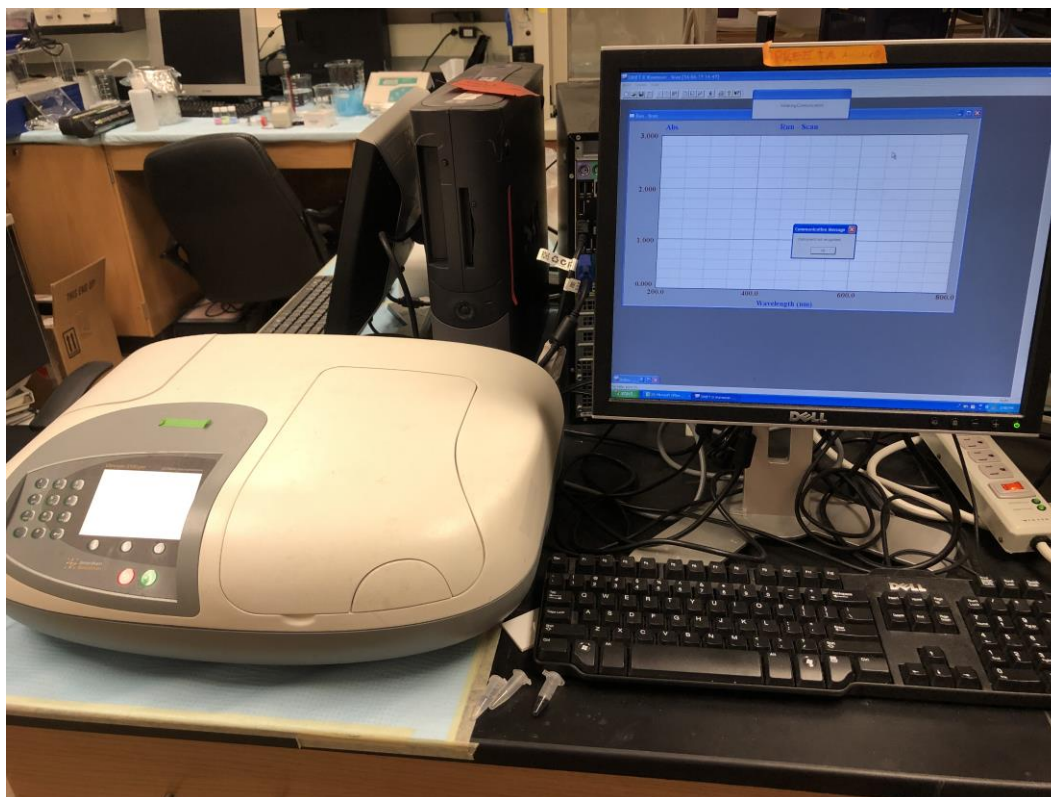


Figure 4-5. Ultraspec 2100pro Ultraviolet–visible spectroscopy

4.2 Synthesis of gold/silver core/shell nanoparticles

4.2.1 Preparation of gold spheres.

First, extracting 10mM HAuCl_4 solution by using syringe. Then fix the syringe in the syringe pump. Adjust the flow speed to $5\mu\text{l}/\text{min}$. The stainless steel will react with the HAuCl_4 when the Au ions go through the needle. Finally, collect the gold solutions and put it in the centrifugal machine (8000 rounds per minute for 6 minutes) to get rid of other metal ions may exist. Remove the supernatant to get the pure gold nanoparticles and add DI water to the same

volume before centrifuge. Then add CTAB (0.1M) in the gold nanoparticles solution to prevent them from aggregation.



Figure 4-6. Accuspin Micro 17 Centrifuge

4.2.2 Synthesis of core/shell nanoparticles by using microfluidic reactor

Two syringes that contain AgNO_3 (1mM) and HAuCl_4 (10mM) separately are connected to two different syringe pumps. Then let the AgNO_3 and HAuCl_4 go through the microfluidic reactor with different flow speed, which can change the different ratios of gold to silver. Afterwards, collect the synthesis

solution in the AA (10mM) solution and adjust the PH by using NaOH (0.01M) to 8. Figure 4-7 shows the assembly device.

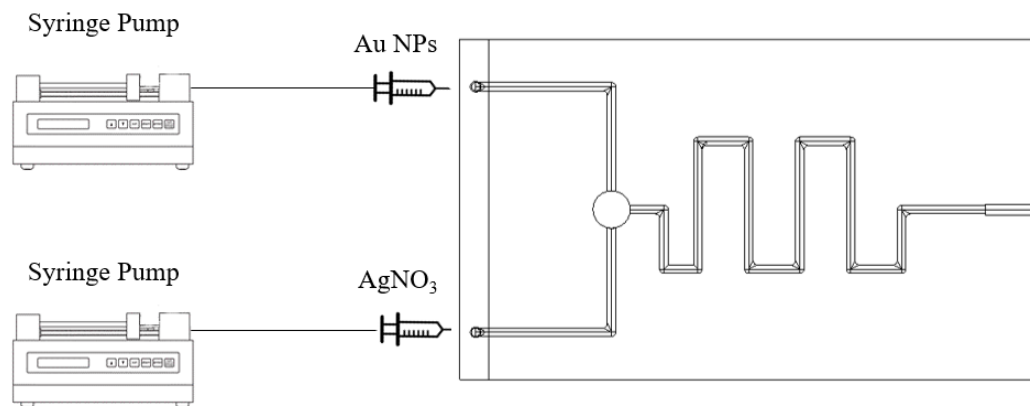


Figure 4-7. Assembly device

4.3 Results and Discussion

In order to get uniform and reliable gold nanoparticles by using stainless-steel needle as reducing agent, we try a lot of different parameters, such as the length of the needle, flow speed, temperature, concentration of the H₂AuCl₄ and PH. Although we can not find the parameters to control the size or distribution of the gold nanoparticles, we still find the best parameter to produce the uniform and reliable gold nanoparticles. When the concentration of 10mM H₂AuCl₄ flow speed arrives 5 μ l/min, and go through the 2 inches needle, we can get pretty good gold nanoparticles. The UVVIS and SEM images shown in the figure 4-8 can prove it. Form the UVVIS image, there is a peak around 538 nanometers. This peak is sharp rather than broad one, which means the size distribution of gold

nanoparticles are uniform. The SEM image proves it too. From the image, the average size of gold nanoparticles is about 60 nanometers and exhibit uniform distribution.

Then we test its stability, the gold nanoparticles are put in the 4°C and 20°C separately. The figure 4-9 shows the UVVIS of the two samples after 4 days. From the UVVIS image, we could find that the stability of the gold nanoparticles is stable in the 4°C, there is nearly no change in the wavelength, absorbance and the naked eye could hardly see the change in the color of the solution. However, in view of the sample at 20°C, although the wavelength doesn't change much, the absorbance and the color of the solution change obviously. The lighter color and lower absorbance indicate that the concentration of the solution will decrease if keep the gold nanoparticles at room temperature. Overall, if the gold nanoparticles could be stored in dark and low temperature environment. It will reveal great stability.

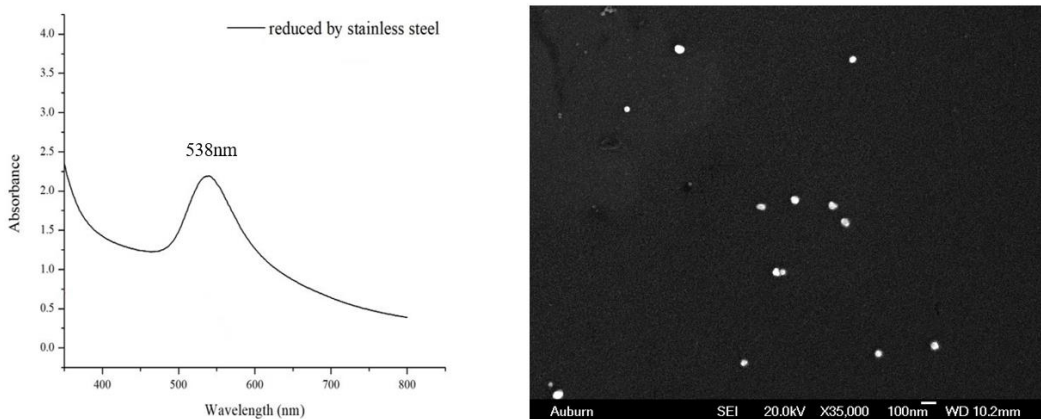


Figure 4-8. The left image is the UVVIS of gold nanoparticles reduced by stainless steel; the right is the SEM image.

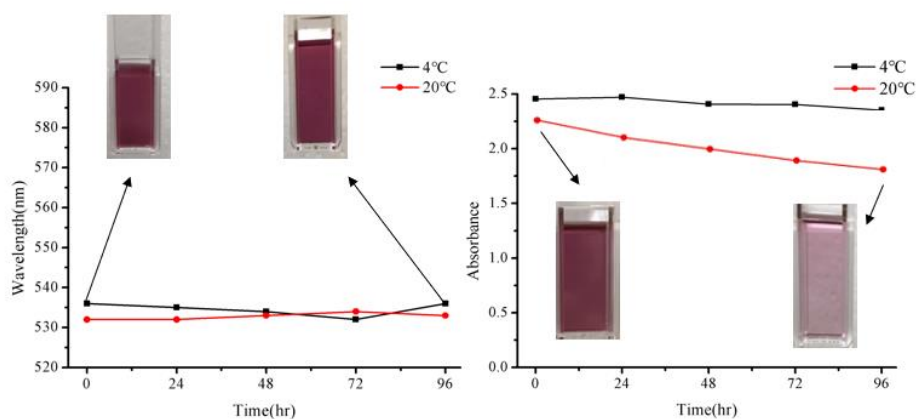


Figure 4-9. Stability test of the gold nanoparticles

In order to control the synthesis process, the microfluidic reactor is printed to apply in the synthesis of the core/shell nanoparticles. As mentioned before, the mass ratio of the gold to silver will affect the size of the core/shell nanoparticles. For controlling the mass ratio easily, the speed of the two inlets are different. It means the injection speed of the AgNO_3 and HAuCl_4 are different. The flow speed of the HAuCl_4 is fixed as $10\mu\text{l}/\text{min}$, also the volume of the HAuCl_4 solution is fixed and when two inlets stop injecting at the same time when the HAuCl_4 solution is exhausted. Then according to change the flow speed of the AgNO_3 solution to achieve the different mass ratios. Because the volume and flow speed of the HAuCl_4 solution is fixed, only change the flow speed can get the same effect that change the volume of the AgNO_3 solution when the concentration of the AgNO_3 and HAuCl_4 are the same.

Figure 4-10 shows the UVVIS images of the core/shell nanoparticles at different mass ratios of the gold to silver. From the figure, we can see that when the mass of the silver increases, the peak around the 530 nm will gradually disappear. Then when the mass of silver continues to increase, the peak will completely disappear around 530 nm. Afterwards, the peak around the 400nm will become higher and sharper. Also, when the mass ratio of gold to silver increases, the blue-shift will appear, it means the wavelength at the peak will decrease. The reason may be due to the mass of silver increase as the mass of gold is fixed, the silver nanoparticles will be coated on the surface of the gold nanoparticles. From the figure we can also see that the small change ratio of gold to silver will lead to the UVVIS image changes a lot.

Figure 4-11 shows the TEM image of the gold/silver core/shell nanoparticles. From the figure, we can see lots of small core/shell nanoparticles. The size is around 20 nm.

For testing the stability of the core/shell nanoparticles, the mass ratio of 6:4 is chosen to keep in the room temperature for one week. The figure 4-12 shows the UVVIS images of the core/shell nanoparticles for one week. From the figure we could see that both the wavelength and absorbance will not be changed a lot. This gold/silver core/shell nanoparticles have good stability.

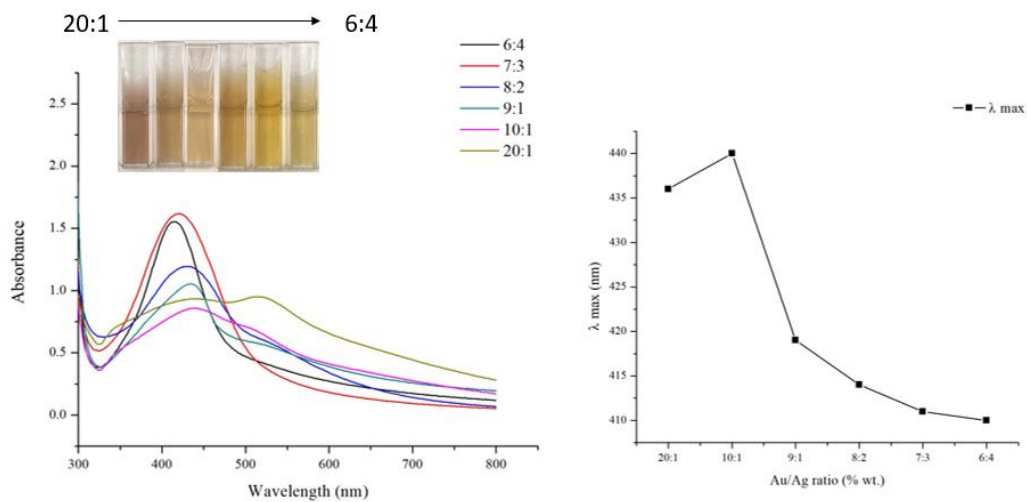


Figure 4-10. UVVIS images of the core/shell nanoparticles at different mass ratios of the gold to silver

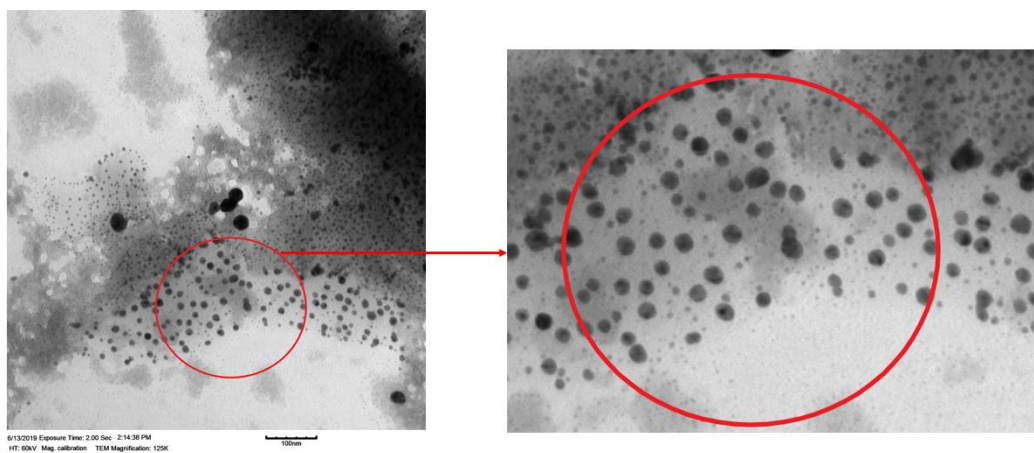


Figure 4-11. TEM image of core/shell nanoparticles

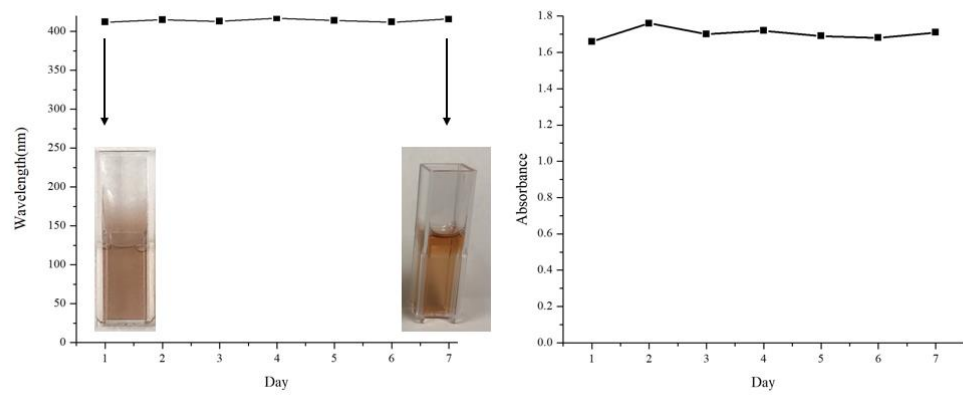


Figure 4-12. Stability test for one week

Chapter 5. Conclusion

In summary, the gold/silver core/shell nanoparticles could be successfully synthesized by using microfluidic reactor. During the synthesis, the microfluidic acts as a reliable and efficient medium that provides the chemical reaction a space to be fully carried out. Its long channel also plays an important role in the reaction. In addition, the microfluidic reactor could be a tool that better control the chemical reaction. The flow of the solution in the channels make the chemical reaction a continuous process, which enables the chemical reaction adequately. The flow speed is important in the microfluidic reactor. According to control the flow speed, the chemical reaction can be easily controlled. Just like the core/shell synthesis, the flow speed can decide the mass ratios of gold to silver. Also, different flow speed can affect the qualities of the products. During the synthesis of BSA/Cu (DDC)₂ NPs, the faster speed can result in better loading efficiency and drug concentration. What's more, the microfluidic can also be used as centrifuge device and produce chemical gradient. Although some more researches should be done to confirm its reliability, the preliminary experiments prove the potential.

In the future, the microfluidics will be more applied in the biology, pharmacology, chemicals and material engineering for its controllable, efficient, rapid and reliable properties. However, there are still some questions for the 3D printed microfluidics.

One is the performance of the 3D printed products; the mechanical strength of most printed composites is still low compared to polymer composites prepared by conventional molding methods and does not meet functional requirements. Therefore, searching or producing new 3D printing materials seem to be a good method. It may be a popular research direction. Another solution to this problem is that people can pre-treat the 3D printing materials so that they can get a better product. But this method may be contradicted with the fast the convenience properties of the 3D printed products. Anyway, there are still challenges for improving the performance of the 3D printed products.

Another is that the 3D printer itself. Right now, there have been lots of kinds of 3D printers. Most of the printing process need lots of time, because if we speed up the process, quality of the products may decrease. How to accelerate the printing process and ensure the quality of the products at the same time has become an interesting challenge.

In general, although there are still many limitations, 3D printing technology develops fast during recent years. In the near future, these problems must be fixed.

References

- [1] Ghosh Chaudhuri, R., & Paria, S. (2011). Core/shell nanoparticles: classes, properties, synthesis mechanisms, characterization, and applications. *Chemical reviews*, 112(4), 2373-2433.
- [2] Oldenburg, S. J., Averitt, R. D., Westcott, S. L., & Halas, N. J. (1998). Nanoengineering of optical resonances. *Chemical Physics Letters*, 288(2-4), 243-247.
- [3] Manisekaran, R. (2018). Literature Survey on Magnetic, Gold, and Core-Shell Nanoparticles. In *Design and Evaluation of Plasmonic/Magnetic Au-MFe₂O₄ (M-Fe/Co/Mn) Core-Shell Nanoparticles Functionalized with Doxorubicin for Cancer Therapeutics* (pp. 37-72). Springer, Cham.
- [4] Gawande, M. B., Goswami, A., Asefa, T., Guo, H., Biradar, A. V., Peng, D. L., ... & Varma, R. S. (2015). Core-shell nanoparticles: synthesis and applications in catalysis and electrocatalysis. *Chemical Society Reviews*, 44(21), 7540-7590.
- [5] El-Toni, A. M., Habila, M. A., Labis, J. P., ALothman, Z. A., Alhoshan, M., Elzatahry, A. A., & Zhang, F. (2016). Design, synthesis and applications of core-shell, hollow core, and nanorattle multifunctional nanostructures. *Nanoscale*, 8(5), 2510-2531.

- [6] Chatterjee, K., Sarkar, S., Rao, K. J., & Paria, S. (2014). Core/shell nanoparticles in biomedical applications. *Advances in colloid and interface science*, 209, 8-39.
- [7] Tan, W., Wang, K., He, X., Zhao, X. J., Drake, T., Wang, L., & Bagwe, R. P. (2004). Bionanotechnology based on silica nanoparticles. *Medicinal research reviews*, 24(5), 621-638.
- [8] De, M., Ghosh, P. S., & Rotello, V. M. (2008). Applications of nanoparticles in biology. *Advanced Materials*, 20(22), 4225-4241.
- [9] Kircher, M. F., Mahmood, U., King, R. S., Weissleder, R., & Josephson, L. (2003). A multimodal nanoparticle for preoperative magnetic resonance imaging and intraoperative optical brain tumor delineation. *Cancer research*, 63(23), 8122-8125.
- [10] Wang, Y., Tang, Z., Correa-Duarte, M. A., Pastoriza-Santos, I., Giersig, M., Kotov, N. A., & Liz-Marzán, L. M. (2004). Mechanism of strong luminescence photoactivation of citrate-stabilized water-soluble nanoparticles with CdSe cores. *The Journal of Physical Chemistry B*, 108(40), 15461-15469.

- [11] Wang, Y., Tu, L., Zhao, J., Sun, Y., Kong, X., & Zhang, H. (2009). Upconversion luminescence of β -NaYF₄: Yb³⁺, Er³⁺@ β -NaYF₄ core/shell nanoparticles: excitation power density and surface dependence. *The Journal of Physical Chemistry C*, 113(17), 7164-7169.
- [12] Qian, H. S., & Zhang, Y. (2008). Synthesis of hexagonal-phase core– shell NaYF₄ nanocrystals with tunable upconversion fluorescence. *Langmuir*, 24(21), 12123-12125.
- [13] Arora, P., Sindhu, A., Dilbaghi, N., & Chaudhury, A. (2011). Biosensors as innovative tools for the detection of food borne pathogens. *Biosensors and Bioelectronics*, 28(1), 1-12.
- [14] Khlebtsov, N., Bogatyrev, V., Dykman, L., Khlebtsov, B., Staroverov, S., Shirokov, A., ... & Terentyuk, G. (2013). Analytical and theranostic applications of gold nanoparticles and multifunctional nanocomposites. *Theranostics*, 3(3), 167.
- [15] Zhong, C. J., & Maye, M. M. (2001). Core–shell assembled nanoparticles as catalysts. *Advanced Materials*, 13(19), 1507-1511.

- [16] Zhang, X. F., Dong, X. L., Huang, H., Lv, B., Zhu, X. G., Lei, J. P., ... & Zhang, Z. D. (2007). Synthesis, structure and magnetic properties of SiO₂-coated Fe nanocapsules. *Materials Science and Engineering: A*, 454, 211-215.
- [17] Xuan, S., Wang, Y. X. J., Yu, J. C., & Leung, K. C. F. (2009). Preparation, characterization, and catalytic activity of core/shell Fe₃O₄@ polyaniline@ Au nanocomposites. *Langmuir*, 25(19), 11835-11843.
- [18] Gross, B. C., Erkal, J. L., Lockwood, S. Y., Chen, C., & Spence, D. M. (2014). Evaluation of 3D printing and its potential impact on biotechnology and the chemical sciences.
- [19] Shallan, A. I., Smejkal, P., Corban, M., Guijt, R. M., & Breadmore, M. C. (2014). Cost-effective three-dimensional printing of visibly transparent microchips within minutes. *Analytical chemistry*, 86(6), 3124-3130.
- [20] Gross, B. C., Erkal, J. L., Lockwood, S. Y., Chen, C., & Spence, D. M. (2014). Evaluation of 3D printing and its potential impact on biotechnology and the chemical sciences.
- [21] Stone, H. A., Stroock, A. D., & Ajdari, A. (2004). Engineering flows in small devices: microfluidics toward a lab-on-a-chip. *Annu. Rev. Fluid Mech.*, 36, 381-411.

- [22] Erkal, J. L., Selimovic, A., Gross, B. C., Lockwood, S. Y., Walton, E. L., McNamara, S., ... & Spence, D. M. (2014). 3D printed microfluidic devices with integrated versatile and reusable electrodes. *Lab on a Chip*, *14*(12), 2023-2032.
- [23] Lee, C. Y., Wang, W. T., Liu, C. C., & Fu, L. M. (2016). Passive mixers in microfluidic systems: A review. *Chemical Engineering Journal*, *288*, 146-160.
- [24] Lee, C. Y., Chang, C. L., Wang, Y. N., & Fu, L. M. (2011). Microfluidic mixing: a review. *International journal of molecular sciences*, *12*(5), 3263-3287.
- [25] Toh, A. G., Wang, Z. P., Yang, C., & Nguyen, N. T. (2014). Engineering microfluidic concentration gradient generators for biological applications. *Microfluidics and nanofluidics*, *16*(1-2), 1-18.
- [26] Francis K, Palsson BO. Effective intercellular communication distances are determined by the relative time constants for cyto/chemokine secretion and diffusion. *Proceedings of the National Academy of Sciences*. 1997 Nov 11;94(23):12258-62.
- [27] Arosio, P., Müller, T., Mahadevan, L., & Knowles, T. P. (2014). Density-gradient-free microfluidic centrifugation for analytical and preparative separation of nanoparticles. *Nano letters*, *14*(5), 2365-2371.

[28] Burger, R., Kirby, D., Glynn, M., Nwankire, C., O'Sullivan, M., Siegrist, J., ... & Ducreé, J. (2012). Centrifugal microfluidics for cell analysis. *Current opinion in chemical biology*, 16(3-4), 409-414.

[29] Morijiri, T., Sunahiro, S., Senaha, M., Yamada, M., & Seki, M. (2011). Sedimentation pinched-flow fractionation for size-and density-based particle sorting in microchannels. *Microfluidics and nanofluidics*, 11(1), 105-110.

[30] Han, T. H., Khan, M. M., Kalathil, S., Lee, J., & Cho, M. H. (2013). Synthesis of positively charged gold nanoparticles using a stainless-steel mesh. *Journal of nanoscience and nanotechnology*, 13(9), 6140-6144.

[31] Song, Y., Hormes, J., & Kumar, C. S. (2008). Microfluidic synthesis of nanomaterials. *small*, 4(6), 698-711.